Validation of Online Scanning-based Linearized IBR Models using Coherence-based Metric

Santosh V. Singh[1], Kaustav Dey[2], Mriganka Mukherjee[1], and A. M. Kulkarni[1]
[1]Department of Electrical Engineering, Indian Institute of Technology Bombay, Mumbai, India
[2]Department of Electrical Engineering, Indian Institute of Technology Kharagpur, Kharagpur, India
Email: santoshvsingh68@gmail.com, kaustav@ee.iitkgp.ac.in, mriganka@iitb.ac.in, anil@ee.iitb.ac.in

***Abstract*—The increasing integration of inverter-based resources (IBRs) in modern power systems has led to a critical need for accurate dynamic models in system stability analysis. However, the proprietary nature of IBR control structures often limits access to these generic models. A widely adopted alternative is the probing-based frequency scanning approach, where the device under test is excited using a small-magnitude, wide-band perturbation signal. The resulting steady-state terminal measurements are used to extract the frequency-domain small-signal model. Despite its popularity, this approach can yield inaccurate models due to measurement noise, insufficient excitation, or nonlinear effects such as controller saturation. This paper proposes a systematic methodology for evaluating the reliability of online scanning–based linearized IBR models using a multi–coherence–based validation index. By examining the complementary coherence function and the variation in the extracted frequency response, it determines whether the current model is trustworthy or corrupted by measurement noise or nonlinearity. The proposed approach is validated using an IBR in the WECC three-IBR test system. The results demonstrate that this approach can effectively identify unreliable small-signal models and enable adjustment of excitation signals, thereby improving the accuracy of online model estimation.**

***Index Terms*—Probing-based system identification, IBR model estimation, frequency scanning, multi-coherence.**

I. Introduction

The proliferation of IBRs, such as renewable energy sources and battery energy storage systems, has transformed the dynamic behaviour of modern power systems. Unlike conventional synchronous machines, IBRs have complex, fast-acting control systems that introduce unique higher frequency control interactions [1]. To analyze and mitigate such interactions, linear time-invariant (LTI) models of the IBR are required, which are valid for small excursions around the equilibrium point. However, such analytical IBR models are not readily provided by the OEMs due to proprietary reasons. As a result, system operators often rely on model identification techniques such as frequency scanning [2], [3] to extract the small-signal model from terminal measurements. In this method, the device under test is perturbed with a small-magnitude, wide-band excitation signal, and the frequency response can be extracted from the steady-state waveforms. This process can also be implemented online, by leveraging nearby voltage source converter (VSC)-based devices as actuators, where the wide-band excitation is injected through reference modulation of the fast inner current control loop [4].

Despite its conceptual simplicity, frequency scanning–based online model extraction faces significant practical challenges. The accuracy of the obtained LTI model strongly depends on the magnitude of the excitation signal, ambient noise, and other parameters [4]. If the perturbation signal is too small, measurement noise dominates, leading to inaccurate estimates. Conversely, if the excitation is too large, the nonlinearities or controller saturations are triggered, violating the small-signal assumption. Additionally, the extent of the response observed at the device terminals also depends on the network characteristics between the point of excitation and the measurement. As a result, predicting the optimal excitation level for such an exercise in a large network is often challenging and requires considerable engineering judgement.

To address this issue, this paper presents a systematic methodology for validating the fidelity of such online scanning–based linearized IBR models. The proposed method utilizes the concept of multi-coherence, which helps to identify whether a certain frequency component in the input and output signals is linearly correlated. The scanning procedure begins with a small-amplitude excitation signal, which is gradually increased. By analyzing the multi-coherence values and the variation in the extracted frequency responses across different excitation levels, the proposed approach determines whether the current model is trustworthy or requires re-excitation with an adjusted amplitude of the excitation signal. The methodology is implemented and tested on a grid-connected IBR in the three-IBR test system [5]. Simulation results demonstrate that the proposed approach can effectively identify unreliable small-signal models and highlight when nonlinearity is excited. The method is expected to facilitate a practical tool for enhancing the reliability of model identification in IBR-dominated grids.

II. Linearized IBR Admittance Model Extraction

If a *black-box* simulation model of an IBR is available, the small-signal frequency response can be numerically obtained using time-domain simulation tools as indicated in Fig. 1. This technique is known as frequency scanning [2], [3]. In this method, the IBR is excited with a wide-band probing signal at its terminals by adding a controlled voltage source. The frequency domain model of the IBR can then be extracted using the steady-state terminal voltage and current waveforms.

979-8-3315-8138-1

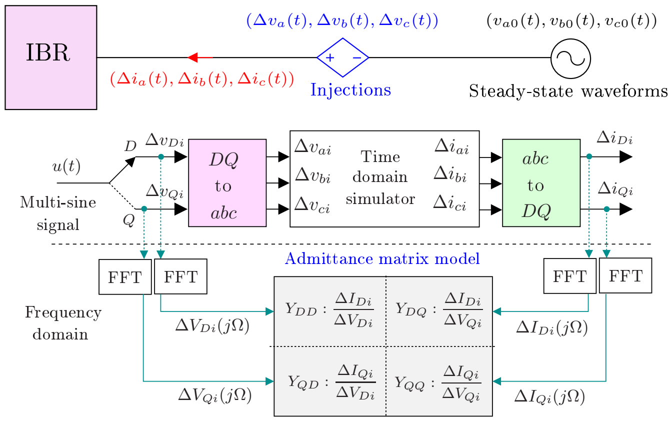

Fig. 1. Estimation of transfer functions using frequency scanning.

Assuming that the excitation signal is sufficiently small to excite the linearized response of the IBR, a multi-sine input of the following form can be used for the frequency scanning.

$$u(t) = \sum_{l=N_1}^{N_2} a_l \sin(2\pi l f_d t + \phi_l) \tag{1}$$

Note that this signal has $N_2 - N_1 + 1$ frequency components (from $N_1 f_d$ to $N_2 f_d$) each spaced by f_d Hz. The magnitude a_l and the phase ϕ_l of the individual components need to be selected appropriately [6] to ensure that the overall magnitude of the multi-sine signal is not very large.

Similar to the simulation-based approach, the small-signal model of an actual IBR can be extracted online (in the field) through tests and measurements when it is in service and is energized. Rather than injecting a multi-sine excitation signal at its terminals, a more convenient and inexpensive way of doing this is to use other VSC-based devices in the vicinity for injecting the signals. Most VSC-based devices typically have a high-bandwidth inner current controller, whose set point can be modulated with multi-sine signals to achieve this. A detailed description of this approach is outlined in [4]. The key aspects of this approach are as follows:
(1) Since the admittance matrix $Y_{DQ}(s)$ of each IBR is a 2×2 matrix, two independent injection scenarios are at least required for this estimation. In practice, these measurements will be corrupted due to ambient noise, measurement errors, and other factors. As a result, additional injection data can be obtained, and a least-squares-type solution can be employed to tackle this problem.
(2) At any nearby IBR, two independent injection scenarios can be generated by using the set-points of the d and q axis variables. However, since more than two injections are preferred, this implies that the overall excitation process cannot be done with a single VSC-based device. The extent of the small-signal response observed at the IBR (under test) terminal due to the multi-sine input depends on the network characteristics between these two devices. Additionally, this characteristic is not fixed but rather depends on the operating conditions and the network topology. Therefore, it is difficult to pre-decide a single excitation amplitude that would work suitably for any device and at any operating condition.

As a result, the amplitude of the multi-sine excitation has to be carefully chosen to ensure that the linearized response of the IBR is accurately captured. In practical systems, the suitability of the applied multi-sine input and the fidelity of the extracted models cannot be determined beforehand, but must be inferred from the recorded measurements themselves. The following section presents the applicability of the "coherence function", which is a commonly used metric for this purpose.

III. Applicability of Coherence Function to Validate Linearity

The coherence function is a normalized index that helps to identify whether the input and output signals at a particular frequency are linearly related. For a system with input $u(t)$ and output $y(t)$, the coherence function $\gamma_{uy}(j\Omega)$ at a frequency Ω rad/s is defined as follows.

$$\gamma_{uy}^2(\Omega) = \frac{|S_{uy}(j\Omega)|^2}{S_{uu}(j\Omega)\, S_{yy}(j\Omega)} \tag{2}$$

where $S_{uy}(j\Omega)$ denotes the cross-power spectral density between $u(t)$ and $y(t)$. If $\mathcal{R}_{uy}(\tau)$ denotes the cross-correlation sequence between $u(t)$ and $y(t)$, then $S_{uy}(j\Omega) = \mathcal{F}(\mathcal{R}_{uy}(\tau))$ where $\mathcal{F}()$ denotes the Fourier transform operation.

The coherence function helps to understand how well the input and the output are correlated at a certain frequency. For example, it is easy to verify that $\mathcal{R}_{uy}(\tau)$ and therefore, $S_{uy}(j\Omega)$ and $\gamma_{uy}^2(j\Omega)$ will be approximately 0 if the output is dominated by uncorrelated white noise. Although the coherence function defined in (2) is valid for scalar inputs and outputs, a formal definition also exists for multi-input output systems, which will be defined later. For the sake of convenience and without loss of generality, the following analysis is presented for the scalar input-output scenario.

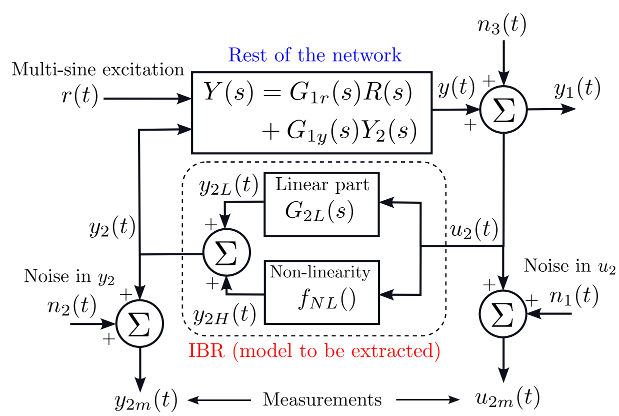

Fig. 2. Schematic of the closed-loop system model

For the probing-based approach discussed in the previous section, the overall power system can be represented as shown in Fig. 2. The network, along with the other devices, is reduced to two inputs: (a) the current injected by the nearby VSC providing the multi-sine excitation, denoted by $r(t)$, and (b) the current injected by the IBR under test, denoted by

979-8-3315-8138-1

$y_2(t)$. The IBR under test, whose model is to be extracted, is represented by a superposition of a linear component $G_{2L}(s)$, which outputs the linearized response of the IBR, and a non-linear component $f_{NL}()$, which outputs the non-linearities due to the excitation input $u_2(t)$. Note that for a sufficiently small input $u_2(t)$, the IBR does not exhibit any perceptible non-linearity, and therefore, can be approximated by the linear block $G_{2L}(s)$ only. The IBR terminal measurements $u_2(t)$ and $y_2(t)$ are superposed with measurement noises $n_1(t)$ and $n_2(t)$, respectively. In addition, the noise source $n_3(t)$ represents the ambient load switching noise. It is assumed that the noise sources are uncorrelated and follow a Gaussian distribution. The small-signal model of the IBR is then estimated using the measured signals $u_{2m}(t)$ and $y_{2m}(t)$, as shown in Fig. 1. The cross-correlation can be represented as follows.

$$\begin{aligned}\mathcal{R}_{uy}(\tau) &= \lim_{T\to\infty}\int_0^T u_{2m}(t)\, y_{2m}(t-\tau)\, dt \\ &= \mathcal{R}_{u_2y_2}(\tau) + \underbrace{\mathcal{R}_{u_2n_2}(\tau) + \mathcal{R}_{y_2n_1}(\tau) + \mathcal{R}_{n_1n_2}(\tau)}_{\approx 0 \text{ since } n_1(t) \text{ and } n_2(t) \text{ are uncorrelated}}\end{aligned}$$

The accuracy of the extracted model and the nature of the coherence function are now presented for different conditions.

A. Excitation $r(t)$ is very small

If the magnitude of $r(t)$ is very small, then the non-linearities can be neglected, and both $u_2(t)$ and $y_2(t)$ will contain the same frequency components as in $r(t)$. However, for very small $r(t)$, the measurements will be as follows.

$$\begin{aligned}u_{2m}(t) &= u_2(t) + n_1(t) \approx n_1(t), \\ y_{2m}(t) &= y_2(t) + n_2(t) \approx n_2(t)\end{aligned}$$

The IBR model $G_{2L}(s)$ cannot be accurately captured since $n_1(t)$ and $n_2(t)$ dominate the measurements. Additionally, since $n_1(t)$ and $n_2(t)$ are uncorrelated, the correlation sequence $\mathcal{R}_{uy}(\tau) \approx 0$. As a result, the coherence function will be $\gamma^2_{uy}(t) \propto |S_{uy}(j\Omega)|^2 \approx 0$. Therefore, the frequency domain model will be erroneous, and the coherence will be very low if the excitation signal magnitude is very small.

B. Excitation $r(t)$ is sufficient

In this case, the magnitude of the excitation $r(t)$ is just sufficient to ensure that the steady-state responses are not dominated by measurement noise, while it is not large enough to excite the non-linear behaviour. Therefore, both $u_2(t)$ and $y_2(t)$ will contain the same frequency components as in $r(t)$. The measured outputs are as follows.

$$u_{2m}(t) \approx u_2(t),\ y_{2m}(t) \approx y_2(t)$$

In this case, $G_{2L}(s)$ can be accurately captured using these measurements $u_2(t)$ and $y_2(t)$. For any excitation frequency Ω rad/s, the corresponding frequency component in $u_2(t)$ and $y_2(t)$ in steady-state will be related by $G_{2L}(j\Omega)$. As a result, $\gamma^2_{uy}(j\Omega) \approx 1$, as expected for correlated frequency components in the input and output signals. Therefore, in this condition, the frequency domain model will be accurate, and the coherence will be ≈ 1.

C. Excitation $r(t)$ is very large to excite IBR non-linearity

In this case, $r(t)$ is large enough to excite the non-linear behaviour (due to f_{NL}) of the IBR. Therefore, the non-linear output $y_{2H}(t)$ can be considered as an additional source of excitation for the frequency components triggered by the IBR non-linearity. Even if $r(t)$ consists of only one frequency input Ω, the non-linear response $y_2(t)$ can contain other frequency components. However, assuming that the rest of the system still operates in the linear range, the new frequency components injected by the IBR will propagate, and in steady-state, will also be present in $u_2(t)$ through the feedback path. Two different injection scenarios are analyzed here.

Only one frequency component Ω injected via $r(t)$: For any frequency Ω_h rad/s that is injected by $y_{2H}(t)$ and not injected by $r(t)$, the corresponding frequency component in the steady-state waveforms of $u_2(t)$ and $y_2(t)$ will be as follows.

$$y_2^h(t) = A\sin(\Omega_h t + \phi_y),\ u_2^h(t) = B\sin(\Omega_h t + \phi_u) \quad (3)$$

where $G_{1y}(j\Omega_h) = \frac{B}{A}\, e^{\,j(\phi_u-\phi_y)}$. As a result, $\gamma^2_{uy}(j\Omega_h) \approx 1$ at frequency Ω_h, even though this frequency was not injected. Therefore, non-zero coherence at any non-injection frequency can be utilized to detect non-linearity, *only* when one frequency is injected at a time.

Multi-sine injected via $r(t)$: If multiple frequencies are injected, even without non-linearity, all these frequency components will be present in $u_2(t)$ and $y_2(t)$. The non-linearity f_{NL} can result in exciting some of these frequency components or some additional components as well. If the same frequency components are excited, they will be due to the superposition of the response due to $r(t)$ and f_{NL}. The presence of correlated frequency components will result in $\gamma^2_{uy}(j\Omega) \approx 1$. For any other frequency Ω_h being excited by the non-linearity, the analysis presented earlier will also hold in this case, which shows that $\gamma^2_{uy}(j\Omega_h) \approx 1$. However, to capture coherence at any other intermediate frequency, it is essential to ensure that the frequency resolution is greater than the fundamental frequency component, which requires that the DFT computation window be longer than one fundamental cycle. In this condition, the extracted small-signal model will be inaccurate due to the non-linearities (depends on the extent of the non-linear behaviour), and the coherence will be ≈ 1.

D. Multi-Coherence Function for Multi Input-Output System

Although the previous analysis was presented for scalar systems, the concept of coherence function extends to multi-input-output systems as well. For the IBR D-Q admittance estimation, Δv_D and Δv_Q are the inputs, and Δi_D and i_Q are the outputs. The multi-coherence function [7] can be evaluated for the outputs, one at a time, as shown in (4).

$$\begin{aligned}{\gamma^2}_{X-i_D}(j\Omega) &= \frac{S^H_{X-i_D}(j\Omega)\, S^{-1}_{X-X}(j\Omega)\, S_{X-i_D}(j\Omega)}{S_{i_D-i_D}(j\Omega)} \\ {\gamma^2}_{X-i_Q}(j\Omega) &= \frac{S^H_{X-i_Q}(j\Omega)\, S^{-1}_{X-X}(j\Omega)\, S_{X-i_Q}(j\Omega)}{S_{i_Q-i_Q}(j\Omega)} \quad (4)\end{aligned}$$

where, $S_{X-X}(j\Omega) = \begin{bmatrix} S_{v_D-v_D}(j\Omega) & S_{v_D-v_Q}(j\Omega) \\ S_{v_Q-v_D}(j\Omega) & S_{v_Q-v_Q}(j\Omega) \end{bmatrix}$;

$$S_{X-i_D}(j\Omega) = \begin{bmatrix} S_{v_D-i_D}(j\Omega) \\ S_{v_Q-i_D}(j\Omega) \end{bmatrix}; \; S_{X-i_Q}(j\Omega) = \begin{bmatrix} S_{v_D-i_Q}(j\Omega) \\ S_{v_Q-i_Q}(j\Omega) \end{bmatrix}.$$

The multi-coherence function for each output lies between 0 and 1. Similar to the scalar case, it equals 1 if a particular frequency component is strongly correlated in any of the inputs and the outputs. If it is significantly below 1, then it indicates that measurement noise is dominant and is responsible for what is observed in the outputs. The multi-coherence function is also expected to be ≈ 1 at a particular frequency if it is excited by a non-linearity.

For n different injection scenarios, there are going to be $2n$ coherence functions (one for Δi_D and one for Δi_Q for each injection). However, it is preferable to have a scalar index rather than comparing $2n$ coherence functions to identify the validity of the extracted model. To achieve this, we propose here the complementary coherence function (CCF), denoted by $\bar{\gamma}^2_{uy}(j\Omega)$, which combines all these coherence functions into one scalar function and is defined as follows.

$$\bar{\gamma}^2_{uy}(j\Omega) = 1 - \prod_{k=1}^{n} \left(\gamma^2_{X-i_{Dk}}(j\Omega) \times \gamma^2_{X-i_{Qk}}(j\Omega) \right) \quad (5)$$

where subscript k denotes the k^{th} injection scenario. Under normal conditions, $\bar{\gamma}^2_{uy}(j\Omega)$ should be ≈ 0 if the coherence functions are ≈ 1. The proposed methodology for identifying the appropriate injection amplitude is now presented.

IV. Proposed Methodology to Identify Unreliable Injection Scenarios

Based on the results in Section III, the characteristics of the extracted model and the CCF can be summarized as follows.
(1) For very low excitation, the measurements are dominated by noise. The frequency responses will be inaccurate, and the CCF is expected to be high (since individual coherence functions are expected to be low).
(2) As the excitation is increased, the effect of measurement noise will reduce, and the accuracy of the frequency response will improve. The CCF will also reduce progressively.
(3) As the excitation magnitude is sufficiently large but non-linearities are not excited, the frequency response will not change much over successive iterations, and CCF ≈ 0.
(4) When $r(t)$ is large enough to excite the non-linearity, the frequency response will again suddenly change (erroneous due to non-linearity), but CCF will still be approximately zero.
The proposed approach utilizes this pattern to identify the optimal injection scenario. The multi-sine magnitude is increased iteratively based on the CCF and the change in the frequency response in successive iterations. The update in the frequency response ΔY (for each term) is evaluated as follows.

$$\Delta Y_{ij} \text{ (in \%)} = \frac{\frac{1}{N_f} \sum \left| Y^k_{ij}(j\Omega) - Y^{k-1}_{ij}(j\Omega) \right|}{\max\left(\left| Y^k_{ij}(j\Omega) \right| \right)} \times 100 \quad (6)$$

where k denotes the current iteration with updated magnitude of excitation and N_f is the number of discrete frequency points over which the estimation is done. Initially, the excitation magnitude should be small enough to ensure that it is operating in the linear range. To achieve this, the initial multi-sine magnitude should be such that the CCF is greater than a pre-determined threshold $\bar{\gamma}^2_{min}$. After this, the excitation

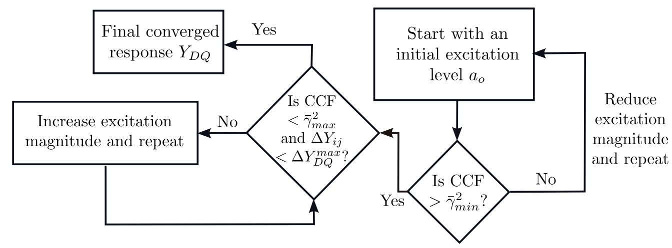

Fig. 3. Proposed algorithm for online frequency response estimation

magnitude should be gradually increased until the CCF is ≈ 0 (falls below a threshold) and the change in the frequency response is lower than a threshold ΔY^{max}_{DQ}. If the change in the admittance matrix had reduced initially but is greater than ΔY^{max}_{DQ} again, this indicates that non-linearities have been excited, and the multi-sine magnitude should be reduced. The key advantage of this approach is its ability to adaptively guide the excitation process, ensuring that the extracted models are both robust against noise and valid within the IBR's linear range. The overall approach is summarized in Fig. 3.

In certain situations, it may be possible that the IBR is operating close to a saturation limit and the algorithm repeatedly fails to find a suitable excitation level. In such a scenario, the algorithm would stop attempting model extraction, flag this condition, and notify the user that a reliable model cannot be extracted under the current conditions. In an online scenario, the estimation methodology would have to wait for an opportune moment when the IBR's operating point has changed, and it can then be re-initiated by the user.

The algorithm relies on two key thresholds: $\bar{\gamma}^2_{min}$ for the CCF and ΔY^{max}_{DQ} for the percentage update in the frequency response. Simulation studies with expected noise levels can help to determine these thresholds for a specific system. The objective is to find a balance where $\bar{\gamma}^2_{min}$ effectively identifies noisy measurements accurately, and ΔY^{max}_{DQ} reliably flags both convergence to the linear model and the onset of non-linearity. For real-world applications, the selection of these thresholds should account for (a) the converter topologies and their associated control strategies, (b) the inherent signal-to-noise ratio of the system under test, and (c) the acceptable level of error or deviation of the extracted models.

V. Simulation Case Studies

To validate the accuracy of this approach, the IEEE 9-bus system with 100% IBR [8], developed on PSCAD [9], is utilized for this study as shown in Figure 4. The IBRs are equipped with outer control loops that determine the set points of the inner current control loop. The small-signal model of IBR 3 is to be estimated here. The current controllers of both IBR 1 and IBR 2 are selected as the excitation points.

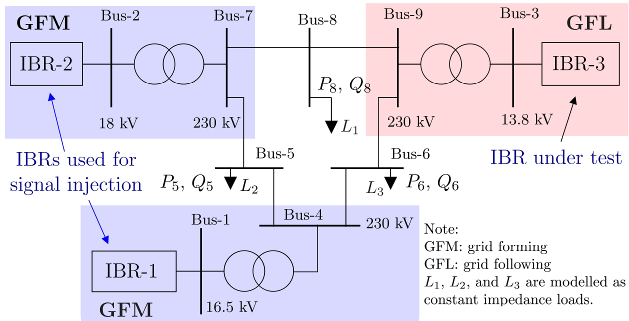

Fig. 4. Schematic of the three-bus IBR-based test system

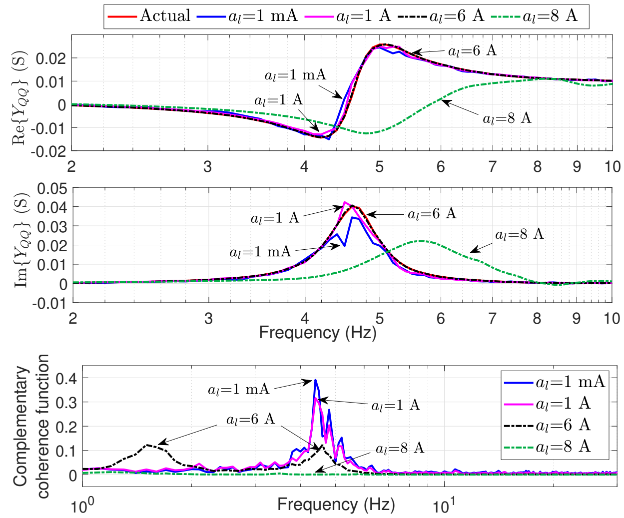

Fig. 5. Estimated Y_{QQ} and CCF with different levels of excitation

The IBR 3 controller is modelled with limiters, which are activated if the injection magnitude exceeds 6 A. The multi-sine signal is constructed with a minimum frequency of 0.1 Hz and up to 100 Hz at a resolution of 0.1 Hz. The measurements for the first 50 s are excluded in each case to allow for the natural transients to decay. Ambient noise is added to the voltage and current measurements at IBR 3 terminals, which are then used to obtain the IBR admittance $Y(j\Omega)$. To assess the accuracy of the estimated model, the frequency response of IBR-3 is obtained using the CPSD method [4] and compared with a reference (true) frequency response obtained under ideal conditions. The error is quantified using the NRMSE index [4].

The model extraction is performed under different levels of multi-sine excitation (magnitude a_l), and the NRMSE errors for all the terms of the 2×2 admittance matrix are shown in Table I. The multi-sine magnitude is gradually increased, and the percentage update ΔY_{ij} is also indicated in the same table. As expected, at a very low excitation level, the NRMSE error is high. As the excitation is increased, the error reduces till about the 6 A case. The percentage update also saturates around this point, indicating that the extracted LTI model is not showing any significant changes. As the excitation is increased further, the NRMSE error starts to increase along with a sudden change in ΔY_{ij}, indicating that non-linearities have been encountered. The frequency response of the Y_{QQ} term (and the CCF) for some of these cases is shown in Fig. 5. As expected, the CCF is higher for very low excitation, and ≈ 0 when the excitation levels are higher. Therefore, the optimal excitation level (which is approximately 6 A) is identified based on the ΔY and the CCF criteria, as outlined in the proposed approach.

TABLE I
NMRSE AND ΔY_{ij} FOR DIFFERENT LEVELS OF MULTI-SINE INJECTION

Amplitude a_l (A)	Metric for Y_{DD} (%)		Metric for Y_{DQ} (%)		Metric for Y_{QD} (%)		Metric for Y_{QQ} (%)	
	NMRSE	ΔY_{DD}	NMRSE	ΔY_{DQ}	NMRSE	ΔY_{QD}	NMRSE	ΔY_{QQ}
0.001	2231.64	-	2367.50	-	2726.63	-	3356.95	-
0.01	1.21	0.05	1.53	0.06	1.47	0.05	1.69	0.06
0.1	1.19	0.52	1.50	0.57	1.46	0.51	1.66	0.62
1	0.97	1.59	1.27	1.68	1.36	1.67	1.42	2.08
2	0.74	0.67	0.60	0.58	0.77	0.71	0.75	0.71
4	0.33	0.55	0.29	0.44	0.40	0.55	0.40	0.55
6	0.17	0.49	0.16	0.38	0.21	0.46	0.23	0.53
8	0.12	46.67	0.11	49.91	0.11	31.04	0.12	42.43

VI. Conclusions and Future Work

This paper presents a systematic methodology for evaluating the reliability of online scanning-based linearized models for IBRs using a coherence-based validation index. By examining the complementary coherence spectra and the variation in the extracted frequency response, the method can distinguish reliable linearized models from those corrupted by measurement noise or non-linearities. The proposed approach is validated using the WECC three-IBR test system. Future research will focus on systematic selection and tuning of update parameters, including excitation amplitude increments, frequency resolution, and the CCF thresholds that govern this process. Although the proposed framework requires further development, the results suggest that it offers a promising direction and has the potential to become a practical tool for online model validation in IBR-rich grids.

References

[1] Y. Cheng, L. Fan, J. Rose, S. H. Huang *et al.*, "Real-world subsynchronous oscillation events in power grids with high penetrations of inverter-based resources," *IEEE Transactions on Power Systems*, vol. 38, no. 1, pp. 316–330, 2022.

[2] X. Jiang and A. Gole, "A frequency scanning method for the identification of harmonic instabilities in HVDC systems," *IEEE Transactions on Power Delivery*, vol. 10, no. 4, pp. 1875–1881, 1995.

[3] A. M. Kulkarni, M. K. Das, and A. M. Gole, "Frequency scanning analysis of STATCOM-network interactions," in *2016 IEEE 6th International Conference on Power Systems (ICPS)*. IEEE, 2016, pp. 1–6.

[4] M. Mukherjee, S. V. Singh, A. Kulkarni, K. Dey, and A. M. Gole, "Online estimation of linearized IBR models using ambient noise and external excitation," *Electric Power Systems Research*, vol. 251, p. 112208, 2026.

[5] R. W. Kenyon, A. Sajadi, A. Hoke, and B.-M. Hodge, "Open-source PSCAD grid-following and grid-forming inverters and a benchmark for zero-inertia power system simulations," in *2021 IEEE Kansas Power and Energy Conference (KPEC)*. IEEE, 2021, pp. 1–6.

[6] R. Pintelon and J. Schoukens, *System identification: a frequency domain approach*. John Wiley & Sons, 2012.

[7] J. S. Bendat and A. G. Piersol, *Random data: analysis and measurement procedures*, 4th ed. John Wiley & Sons, 2011.

[8] R. W. Kenyon, A. Sajadi, A. Hoke, and B.-M. Hodge, "Open-source PSCAD grid-following and grid-forming inverters and a benchmark for zero-inertia power system simulations," in *2021 IEEE Kansas Power and Energy Conference (KPEC)*. IEEE, 2021, pp. 1–6.

[9] 2010, Manitoba HVDC Research Centre, PSCAD/EMTDC Users guide, Winnipeg, Canada.

979-8-3315-8138-1